This journal is © The Royal Society of Chemistry 2012

Supplementary Material

Enhanced bistability by guest inclusion in Fe(II) spin crossover porous coordination polymers

Francisco J. Muñoz Lara,[a] Ana B. Gaspar,[a] Daniel Aravena,[b] Eliseo Ruiz,[b] M. Carmen Muñoz[c], Masaaki Ohba[d], Ryo Ohtani[e], Susumu Kitagawa[e,f] and José A. Real[*a]

[a] *Institut de Ciència Molecular/Departament de Química Inorgánica, Universitat de València, Edifici d'Instituts de Paterna, Carrer Catedràtic José Beltrán Martínez 2, 46980 Paterna, València, Spain.*

[b] *Departament de Química Inorgànica and Institut de Recerca de Química Teòrica i Computacional, Universitat de Barcelona, Diagonal 645, Barcelona 08028 Spain.*

[c] *Departament de Física Aplicada, Universitat Politècnica de València, Camí de Vera s/n, 46022 València, Spain.*

[d] *Department of Chemistry, Faculty of Science, Kyushu University, Hakozaki 6-10-1, Higashi-ku, Fukuoka 812-8581, Japan.*

[e] *Department of Synthetic Chemistry and Biological Chemistry, Graduate School of Engineering, Kyoto University, Katsura, Nishikyo-ku, Kyoto 615-8510, Japan.*

[f] *Institute for Integrated Cell-Material Sciences (iCeMS), Kyoto University, Yoshida, Sakyo-ku, Kyoto 606-8501, Japan.*

Electronic Supplementary Information (ESI) available: Experimental section, crystallographic data, thermogravimetric analysis, study of the thermal hysteresis cycles at different measurement rates, magnetic properties of microcrystalline powder of **1**, plots of $\chi_M T$ vs T together with the derivatives for **1** and **2** and magnetic properties of **2'**. DSC measurements between 300 -700 K. Computational details, density of states of the low- and high-spin states of the clathrate $[Fe(pz)Pt(CN)_4]\cdot 0.5(CS(NH_2)_2)$, optimized lattice parameters (in Å and degrees) and bond distances involving the transition metal atoms optimized structures of the high- and low-spin of clathrate $[Fe(pz)Pt(CN)_4]\cdot 0.5(CS(NH_2)_2)$ using the Siesta code with the PBEsol funcional and a numerical doble-ζ basis set and pseudopotentials, projected DOS and COD (integrated COD – ICOD) curves.

Experimental section

Physical characterization. Variable-temperature magnetic susceptibility measurements of samples (20–30 mg microcrystals) were recorded at the rate of 2 K/min with a Quantum Design MPMS2 SQUID susceptometer equipped with a 5.5 T magnet, operating at 1 T and at temperatures from 1.8–400 K. The susceptometer was calibrated with $(NH_4)_2Mn(SO_4)_2 \cdot 12H_2O$. Experimental susceptibilities were corrected for diamagnetism of the constituent atoms by the use of Pascal's constants. Calorimetric measurements have been performed using a differential scanning calorimeter (Mettler Toledo DSC 821e). Low temperatures were obtained with an aluminium block which was attached to the sample holder, refrigerated with a flow of liquid nitrogen, and stabilized at a temperature of 110 K. The sample holder was kept in a drybox under a flow of dry nitrogen gas to avoid water condensation. The measurements were carried out using around 20 mg of a powdered sample sealed in aluminium pans with a mechanical crimp. Temperature and heat flow calibrations were made with standard samples of indium by using its melting (429.6 K, 28.45 J g^{-1}) transition. An overall accuracy of 0.2 K in the temperature and 2% in the heat flow is estimated. The thermodynamic parameters were analyzed with Netzsch Proteus software (NETZSCH-Geraetebau GMBH). IR spectra were recorded at 293 K in KBr using a Nicolet 5700 FTIR spectrometer. TGA measurements were performed on a Mettler Toledo TGA/SDTA 851e, in the 300-700 K temperature range in nitrogen atmosphere with a rate of 10 K/min. Microanalysis was done by using PV 9760 EDAX Microanalysis with a PHILIPS XL 30 ESEM scanning electron microscope.

Single crystal X-ray diffraction. Diffraction data was collected with a Nonius Kappa-CCD single crystal diffractometer using Mo-K_α radiation (λ = 0.71073 Å). The structures were solved by direct methods using SHELXS-97 and refined by full-matrix least-squares on F^2 using SHELXL-97.[1] All non-hydrogen atoms were refined anisotropically. CCDC 859774, 859775 and 864040 (**1** at 250 K) contains the supplementary crystallographic data for compounds **1** and **2**. This data can be obtained free of charge from The Cambridge Crystallographic Data Centre via www.ccdc.cam.ac.uk/data_request/cif.

1. G. M. Sheldrick, SHELX97, Acta Cryst. A64, 112-122, 2008.

Materials. Starting reagents and solvents were obtained commercially from Aldrich or Across and used as received.

Synthesis of $[Fe(pz)Pt(CN)_4]\cdot 0.5(CS(NH_2)_2)$ (1) and $[Fe(pz)Pd(CN)_4]\cdot 1.5H_2O\cdot 0.5(CS(NH_2)_2)$ (2). Single crystals of **1** and **2** were grown using a slow diffusion technique. One side of a multi-arm shaped vessel contains $(NH_4)_2Fe(SO_4)_2\cdot 6H_2O$ (0.127 mmol, 50 mg) dissolved in water (0.5 mL). The contiguous arms contain water solutions (0.25 mL) of pyrazine (0.153 mmol, 12.25 mg) and of $K_2M(CN)_4\cdot nH_2O$ (Pt: 0.127 mmol, 55 mg, 0.5 mL, n = 3; Pd: 0.127 mmol, 36.8 mg, 0.5 mL, n = 1). The vessel was filled with a water solution containing 0.5 g of thiourea. Prismatic yellow (**1**) and orange (**2**) crystals suitable for single crystal X-ray analysis were obtained after 3 weeks.

Anal. Calc. for **1**: $C_{8.5}H_6N_7S_{0.5}FePt$: C, 21.58; H, 1.28; N, 20.72; S, 3.39. Found: C, 20.26; H, 1.88; N, 19.77; S, 4.02. EDAX calc. for **1**: Fe:Pt (50:50); exp: Fe, 49.6; Pt, 50.4.

Anal. Calc. for **2**: $C_{8.5}H_9N_7S_{0.5}O_{1.5}FePd$: C, 24.81; H, 2.20; N, 23.83; S, 3.90. Found: C, 23.25; H, 2.42; N, 22.54; S, 4.18. EDAX calc. for **2**: Fe:Pd (50:50); exp: Fe, 49.8; Pd, 50.2.

Synthesis of $[Fe(pz)Pd(CN)_4]\cdot 0.5(CN_2H_4S)$ (2'). Compound **2'** has been obtained by heating at 160°C during 24 hours compound **2**. Thermo gravimetric analysis performed on **2'** has demonstrated that the dehydration was complete.

Anal. Calc. for **2'**: $C_{8.5}H_6N_7S_{0.5}FePd$: C, 26.55; H, 1.57; N, 25.50; S, 3.96. Found: C, 26.15; H, 1.61; N, 25.57; S, 4.18. EDAX calc. for **2'**: 50:50; exp: Fe, 49.8; Pd, 50.2.

STable 1. Crystal data for **1** and **2**.

	1	**1**	**2**
T (K)	120	250	120
Empirical formula	$C_{8.5}H_6N_7FePtS_{0.5}$	$C_{8.5}H_6N_7FePtS_{0.5}$	$C_{8.5}H_6N_7FePdS_{0.5}$
*M*r	473.17	473.17	384.48
Crystal system	tetragonal	tetragonal	tetragonal
Space group	P 4/mmm	P 4/mmm	P 4/mmm
a (Å)	7.1910(4)	7.4564(3)	7.2070(12)
c (Å)	6.8020(4)	7.2671(9)	6.798(3)
V (Å^3)	351.73(3)	404.04(6)	353.09(15)
Z	1	1	1
D_c (mg cm^{-3})	2.234	1.945	1.808
F(000)	218	218	186
μ (Mo-K$_\alpha$) (mm^{-1})	0.71073	0.71073	0.71073
Crystal size (mm)	0.06x0.02x0.02	0.06x0.02x0.02	0.04x0.02x0.02
No. of unique reflections	378	357	401
No. of reflections [$I>2\sigma(I)$]	377	338	198
R_1 [$I>2\sigma(I)$]	0.0260	0.0520	0.0485
wR [$I>2\sigma(I)$]	0.0620	0.1106	0.1120
S	1.086	1.027	0.894

$R_1 = \Sigma \, ||Fo| - |Fc|| \, / \, \Sigma \, |Fo|$; $wR = [\Sigma \, [w(Fo^2 - Fc^2)^2] \, / \, \Sigma \, [w(Fo^2)^2]]^{1/2}$;

$w = 1/ \, [\sigma^2(Fo^2) + (m \, P)^2 + n \, P]$ where $P = (Fo^2 + 2Fc^2) \, / \, 3$;

m = 0.0422 (**1**, 120 K), 0.0773 (**1**, 250 K) and 0.1077 (**2**); n = 0.0000 (**1**, 120 K), 0.0000 (**1**, 250 K) and 12.5688(**2**).

STable 1cont. Selected bond lengths [Å] and angles [°] for **1** and **2**.

	1	**1**	**2**
	120 K	**250 K**	**120 K**
Fe-N(1)axial	1.999(7)	2.23(2)	2.011(13)
Fe-N(2)equatorial	1.939(6)	2.134(14)	1.943(10)
N(3)-C(3)	1.451(10)	1.53379(12)	1.447(10)
C(3)-S	1.650(10)	1.7109	1.644(10)
N(3)-C(3)-S	127.8(13)	126.892(4)	131.2(17)
N(3)-C(3)-N(3)	104(3)	106.216(7)	98(3)

This journal is © The Royal Society of Chemistry 2012

STable 2. Crystal data for **1** and **2** at 320 K and 295 K, respectively.

	1	**2**
T (K)	320	295
Empirical formula	$C_{8.5}H_6N_7FePtS_{0.5}$	$C_{8.5}H_6N_7FePdS_{0.5}$
*M*r	473.17	384.48
Crystal system	tetragonal	tetragonal
Space group	P 4/mmm	P 4/mmm
a (Å)	7.42(6)	7.471(3)
c (Å)	7.25(5)	7.246(13)
V (Å^3)	399.2(6)	404(1)

STable 3. Intermolecular contacts between the framework and guest molecules in **1** (120 K and 250 K) and **2** (120 K).

120 K (LS state)	**1**	**2**
C(2)···N(3)	3.44(2)	3.48(2)
C(1)···N(3)	3.794(4)	3.797(6)
C(1)···C(3)	3.666(4)	3.676(3)
N(1)···N(3)	3.605(2)	3.616(3)
N(2)···N(3)	3.45(2)	3.49(2)
S···Pt	3.561(8)	
S···Pd		3.544(9)
S···C(2)	3.698(3)	3.700(5)

250 K (HS state)	**1**
C(2)···N(3)	3.628(7)
C(1)···N(3)	3. 928(8)
C(1)···C(3)	3.800(6)
N(1)···N(3)	3.733(2)
N(2)···N(3)	3.605(7)
S···Pt	3.795(4)
S···C(2)	3.908(4)

SFigure 1. View of a fragment of **1** and **2** along *y* (top) and *z*-directions (bottom). Due to substitutional disorder the invited thiourea molecule appears like an infinite system of chains running along *x* and *y* directions. Given that only one of the two orthogonal distributions is possible and taking into account that the occupation factor of the invited molecule of thiourea is 0.5 a picture of the framework consistent with the stoichiometry is shown in Fig. 1 of the manuscript.
Colour code: Iron (orange), platinum (pink), nitrogen (blue) and carbon (grey), nitrogen guest molecule (green), C guest molecule (black) and S guest molecule (yellow).

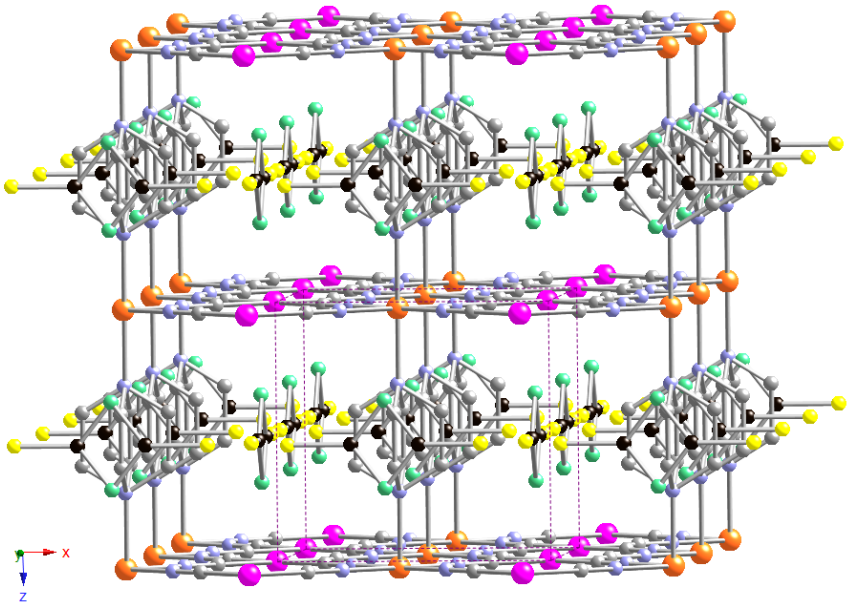

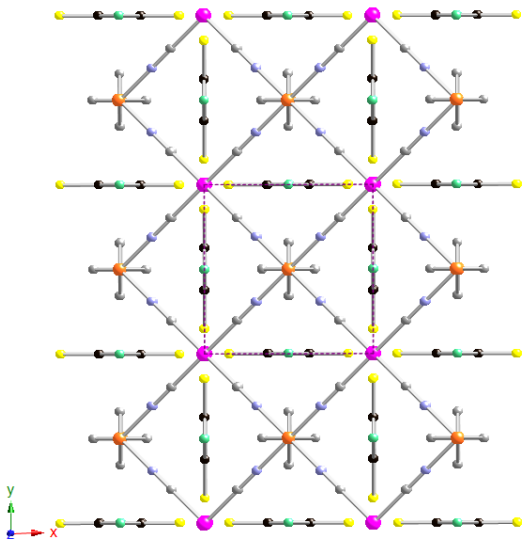

SFigure 2. View of the intermolecular contacts (red dotted lines) between the framework and guest molecules in **1** and **2**.

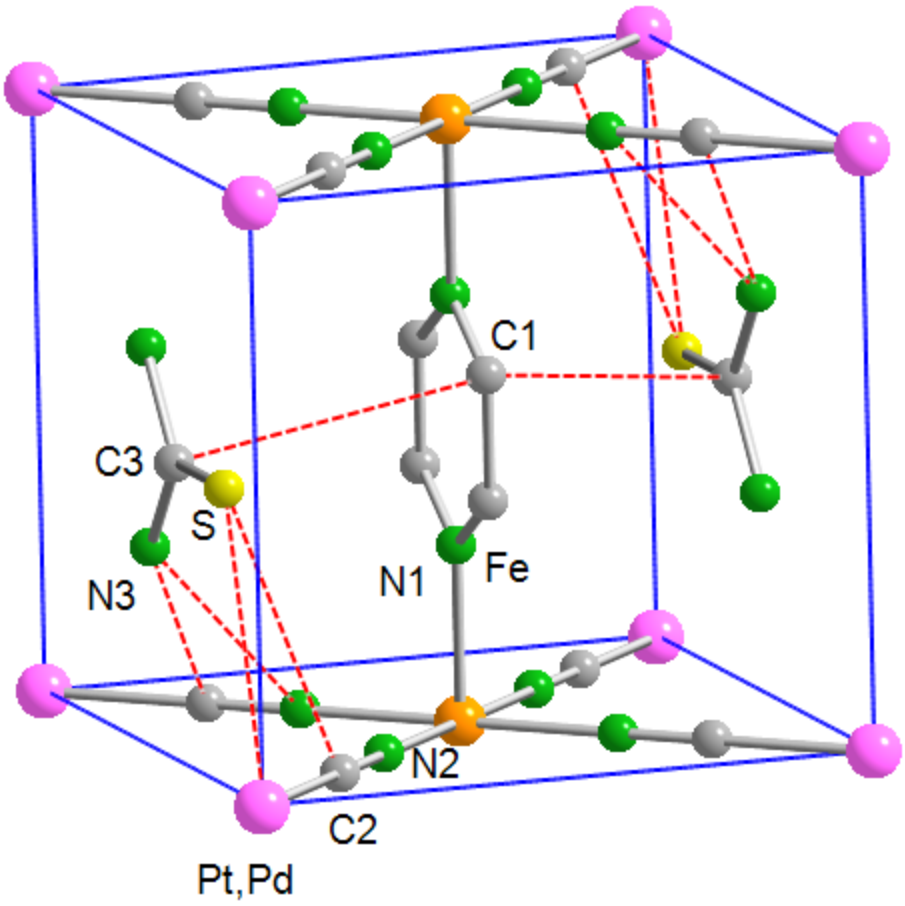

SFigure 3. Thermal gravimetric analysis of **1**, **2** and **2'**.

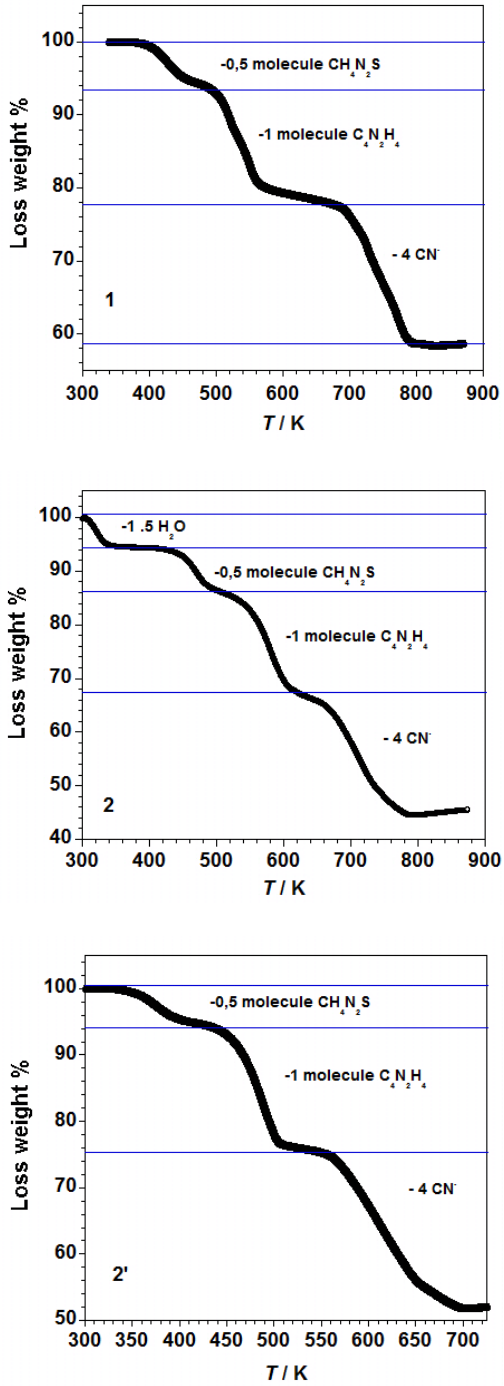

SFigure4. Study of the thermal hysteresis cycle in **1**.

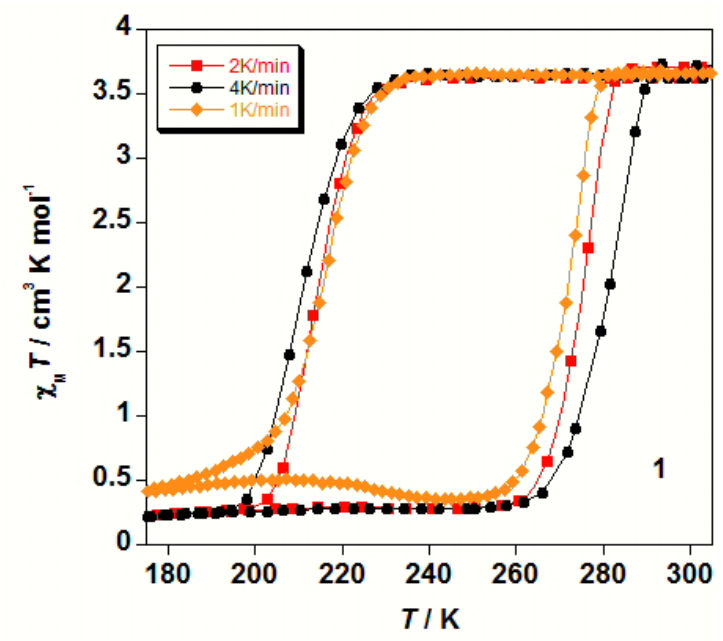

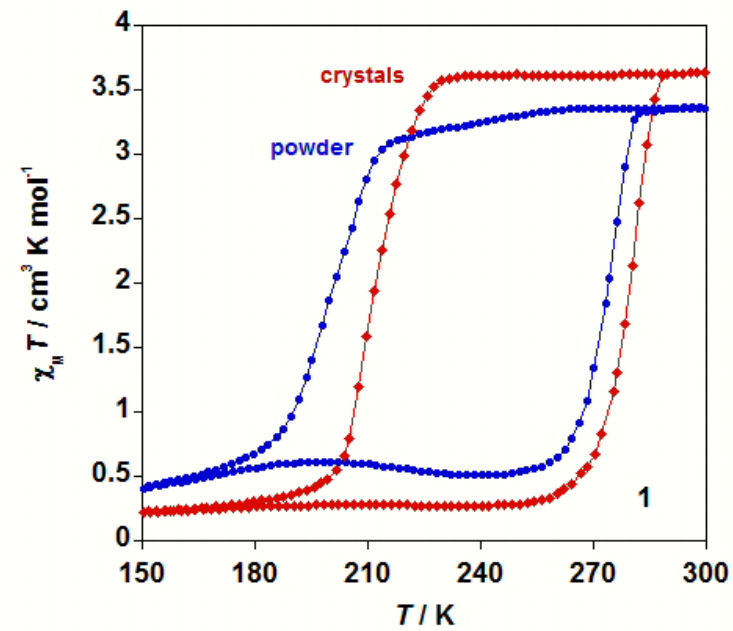

SFigure5. Study of the thermal hysteresis cycle in **2**.

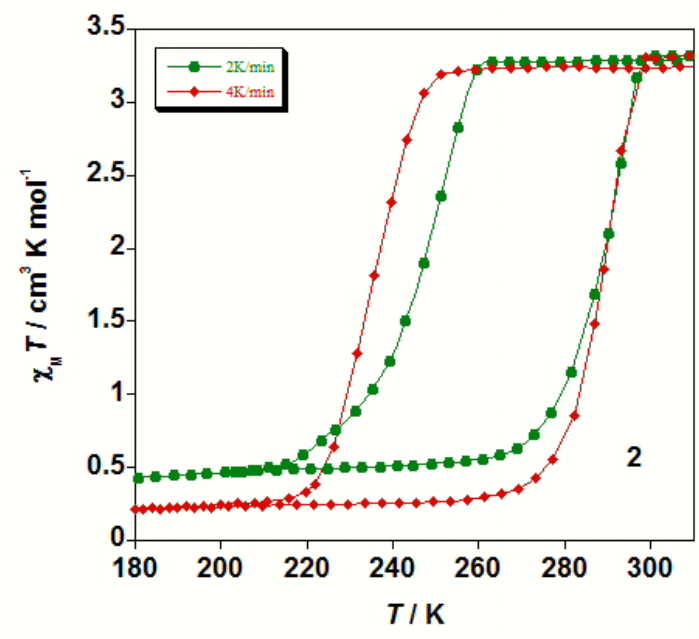

SFigure6. Magnetic properties of **1** and **2** in the form of $\chi_M T$ vs T and the corresponding derivatives in the cooling (red) and warming (blue) modes.

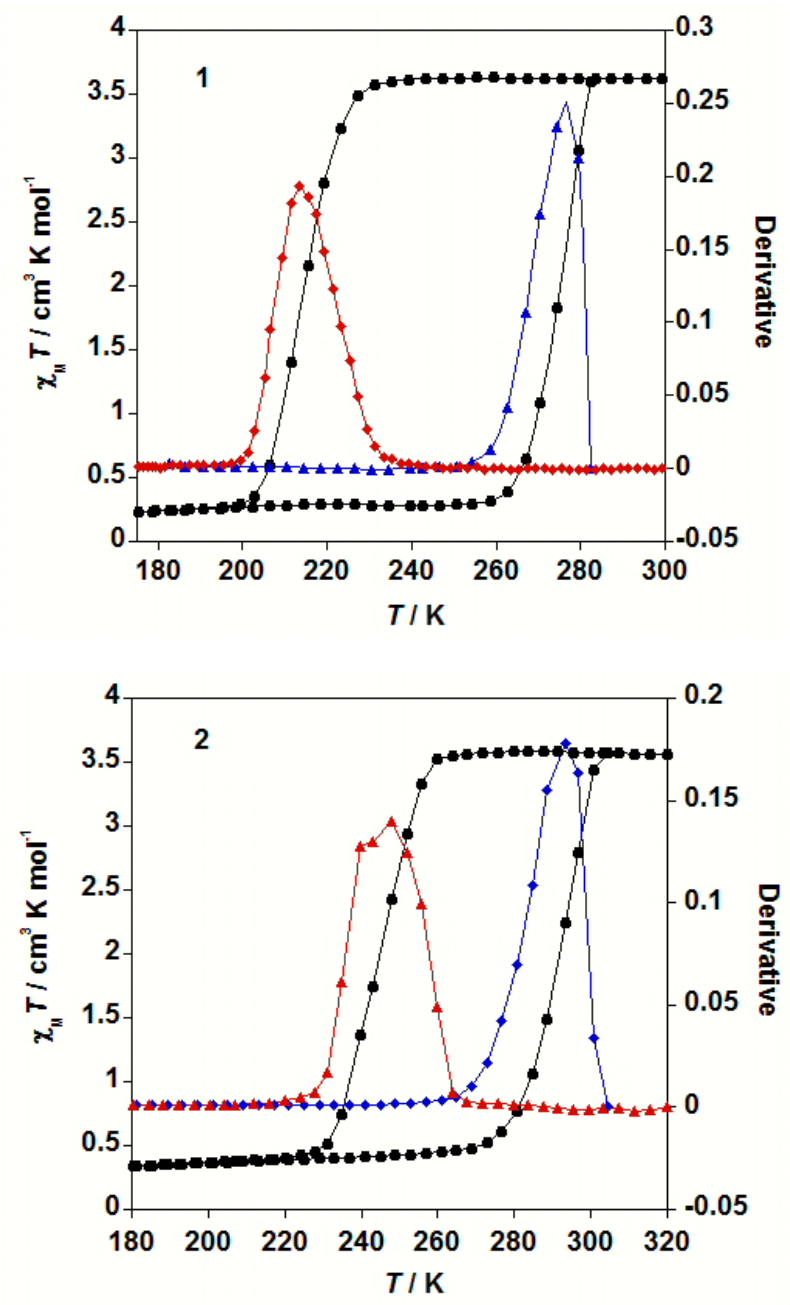

SFigure7. Magnetic properties of **2** and **2'** in the form of $\chi_M T$ vs T.

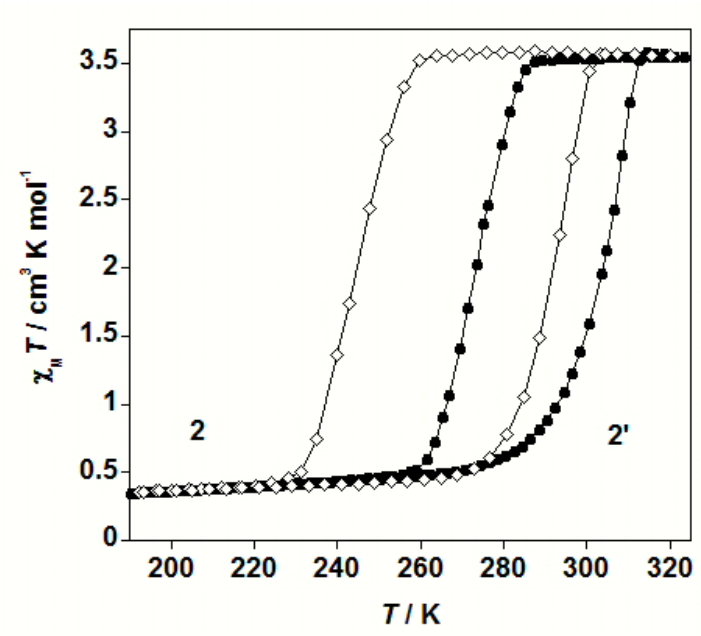

SFigure8. Thermal dependence of the anomalous molar specific heat (ΔCp) for **1** and **2** deduced from the differential scanning calorimetry measurements. The different anomalies observed for each mode may reflect changes in cooperativity related to subtle structural modifications occurring during the spin state change and have also been detected from the derivative of $\chi_M T$ vs T (SFig.6). The critical temperatures of the spin transition deduced from this experiment are: $T_c^{\downarrow}$ = 220 K (**1**) and 246 K (**2**); $T_c^{\uparrow}$ = 273 K (**1**) and 293 K (**2**). These values agree pretty well with those deduced from magnetism.

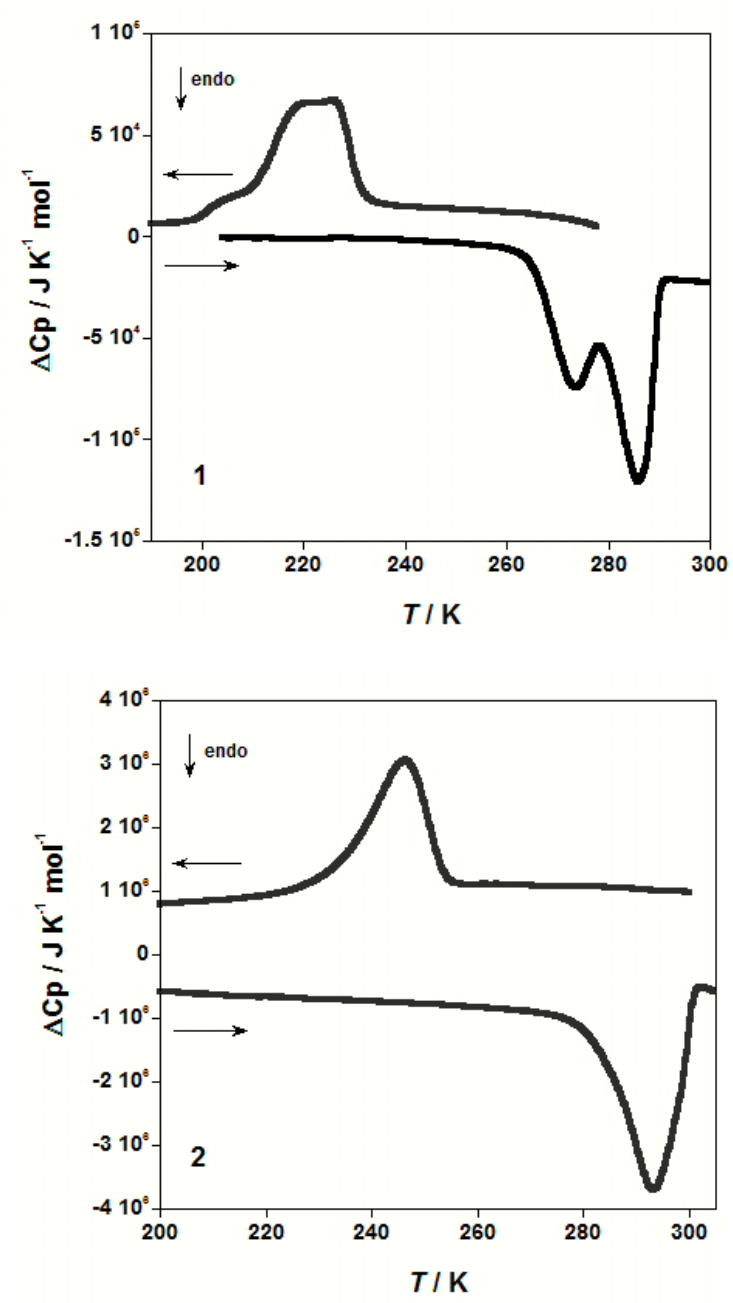

Computational Details

Full optimisation of the low- and high-spin states of the $\{Fe(pz)[Pt(CN)_4]\}\cdot 0.5(CS(NH_2)_2)$ compound was performed by means of Density Functional Theory[1] calculations using the Siesta code.[2] For such calculations, the PBEsol functional[3] was employed because it provides a better agreement with the available experimental crystal structure than other functionals, such as PBE[4]. Only valence electrons are included in the calculations, with the core being replaced by norm-conserving scalar relativistic pseudopotentials factorized in the Kleinman-Bylander form.[5] The pseudopotentials are generated according to the method proposed by Trouiller and Martins.[6] Using the following cutoff radii for the s, p, d and f shells: Pt ($6s^1$ r=2.32 $6p^0$ r=2.47 $5d^9$ r=1.23 $5f^0$ r=2.32), Pd ($5s^1$ r=3.11 $5p^0$ r=2.67 $4d^9$ r=2.25 $5f^0$ r=2.67), Fe ($3s^2$ r=1.54 $3p^6$ r=2.05 $3d^6$ r=1.64 $4f^0$ r=2.05), S ($3s^2$ r=1.69 $3p^4$ r=1.69 $3d^0$ r=1.69 $4f^0$ r=1.69), O($2s^2$ r=1.14 $2p^3$ r=1.14 $3d^0$ r=1.14 $4f^0$ r=1.14), N ($2s^2$ r=1.14 $2p^3$ r=1.14 $3d^0$ r=1.14 $4f^0$ r=1.14), C($2s^2$ r=1.25 $2p^2$ r=1.25 $3d^0$ r=1.25 $4f^0$ r=1.25) and H ($1s^1$ r=1.14 $2p^0$ r=1.14 $3d^0$ r=1.14 $4f^0$ r=1.14). As basis set a double- ζ with polarization was employed for the S, O, N, C and H while for Pt (Pd) atoms a double-ζ for the 6s (5s) and 5d (4d) orbitals and single- ζ for the 6p (5p) ones, and for the iron atoms single-ζ quality for the 3s, 3p and 4p orbitals and double-ζ quality for the 3d and 4s ones. There are two parameters that control the accuracy of the numerical calculations: i) since the wavefunction vanishes at the chosen confinement radius r_c, whose value is different for each atomic orbital, the energy radii of different orbitals is determined by a single parameter, *the energy shift*, which is the energy increase of the atomic eigenstate due to the confinement and ii) the integrals of the self-consistent terms are obtained with the help of a regular real space grid in which the electron density is projected. The grid spacing is determined by the *maximum kinetic energy* of the plane waves that can be represented in that grid. We have employed in the calculations an *energy shift* of 50 meV and *maximum kinetic energy* value of 250 Ry.

References

1 R. M. Martin, *Electronic Structure, Basic Theory and Practical Methods*, Cambridge University Press, Cambridge, 2004.

2 J. M. Soler, E. Artacho, J. D. Gale, A. García, J. Junquera, P. Ordejón, D. Sánchez-Portal, *J. Phys.: Condens. Matter* **2002**, 14, 2745.; D. Sánchez-Portal, P. Ordejón, E. Artacho, J. M. Soler, *Int. J. Quant. Chem.* **1997**, 65, 453.

3 J.P. Perdew, A. Ruzsinszky, G. I. Csonka, O. A. Vydrov, G. E. Scuseria, L. A. Constantin, X. Zhou, and K. Burke, *Phys. Rev. Lett.* **2008**, *100*, 136406.

4 J. Perdew, K. Burke, M. Ernzerhof, *Phys. Rev. Lett.* **1996**, 77, 3865.

5 L. Kleinman, D. M. Bylander, *Phys. Rev. Lett.* **1982**, *48*, 1425.

6 N. Trouiller, J.L. Martins, *Phys. Rev. B* **1991**, *43*, 1993.

STable4. Optimized lattice parameters (in Å and degrees) and bond distances involving the transition metal atoms optimized structures of the high- and low-spin of clathrate $\{Fe(pz)[X(CN)_4]\}\cdot 0.5(CS(NH_2)_2)$ (X = Pt or Pd) using the Siesta code with the PBEsol funcional and a numerical doble-ζ basis set and pseudopotentials. Available experimental values of low-spin state are provided for comparison.

	a	b	c	α	β	γ	d(Fe-NC)	d(Fe-Npz)	d(X-CN)
X = Pd									
Opt HS	7.078	7.383	7.566	90.0	90.0	90.1	2.112	2.126	1.986
Opt LS	6.760	7.133	7.237	90.0	90.0	90.1	1.903	1.964	1.994
Exp LS	6.798	7.207	7.207	90.0	90.0	90.0	1.939(6)	1.999(7)	1.991(7)
X = Pt									
Opt HS	7.092	7.318	7.578	90.0	90.0	90.1	2.112	2.134	1.974
Opt LS	6.766	7.090	7.238	90.0	89.9	90.1	1.903	1.966	1.977
Exp LS	6.800	7.190	7.190	90.0	90.0	90.0	1.941	1.996	1.980

SFigure9. Density of States of the low- and high-spin states of the clathrate $\{Fe(pz)[Pt(CN)_4]\}\cdot 0.5(CS(NH_2)_2)$.

alpha and beta density of states low-spin state

Fermi level –4.7 eV

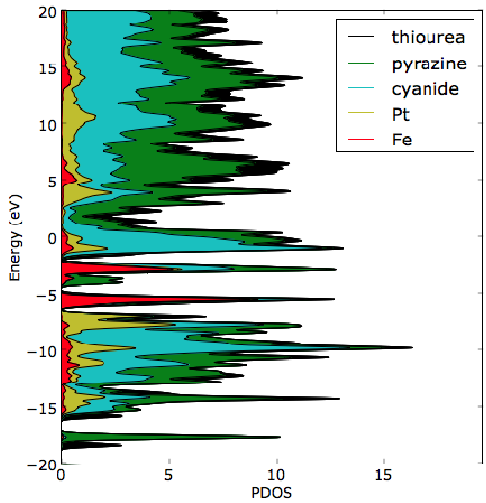

alpha density of states high-spin state

beta density of states high-spin state

Fermi level –4.7 eV

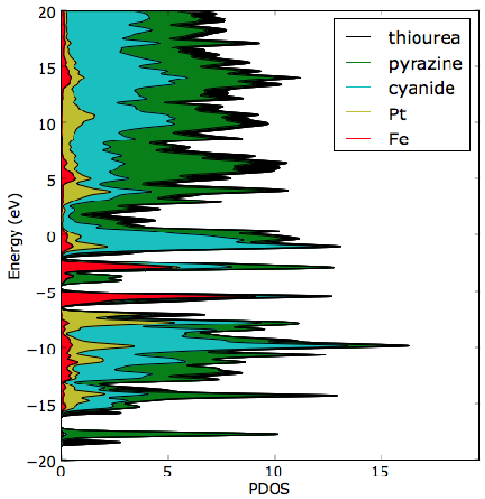

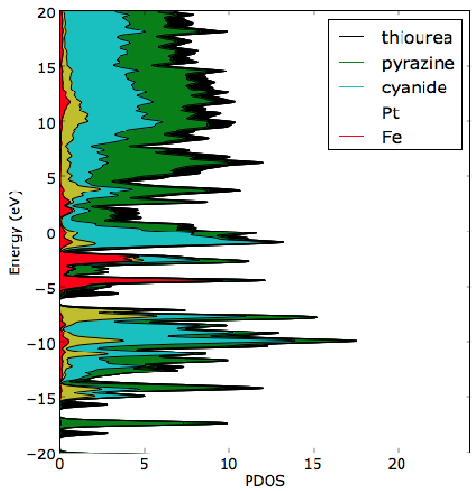

SFigure10 Projected DOS and COD (integrated COD – ICOD) curves for Pt atoms of the host lattice, S atoms of the thiourea and the CN groups of the host lattice for the low- and high-spin states of the $\{Fe(pz)[Pt(CN)_4]\}\cdot 0.5(CS(NH_2)_2)$ clathrate . The COD curves correspond to the difference of the projected DOS between the isolated host and guest systems (first figure) and the host···guest system (second figure).

alpha and beta projected DOS and COD-ICOD curves of the low-spin state (Fermi level –4.7 eV)

isolated host and guest host···guest Pt S CN

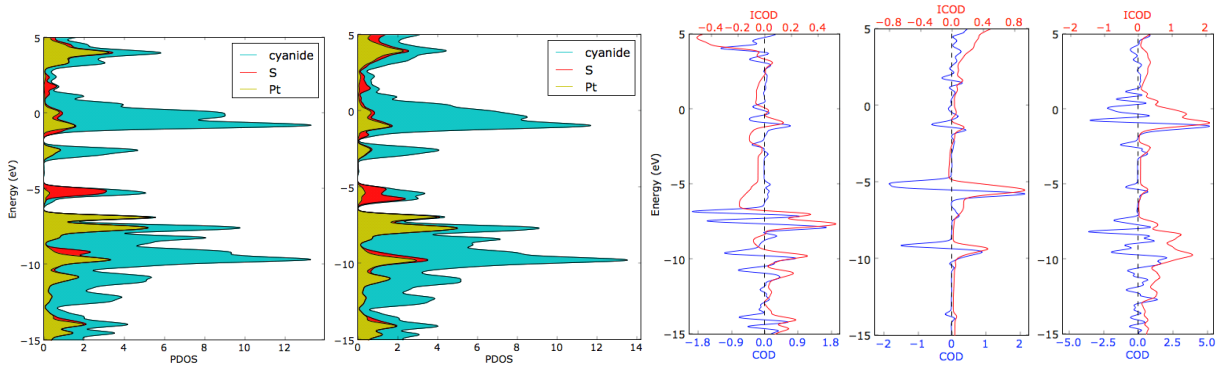

alpha projected DOS and COD-ICOD curves of the high-spin state (Fermi level –4.7 eV)

isolated host and guest host···guest Pt S CN

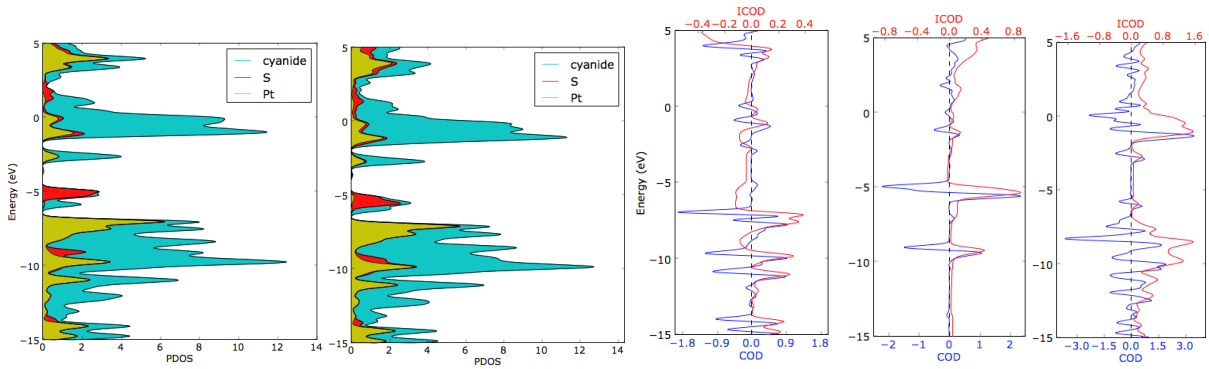

beta projected DOS and COD-ICOD curves of the high-spin state (Fermi level –4.7 eV)
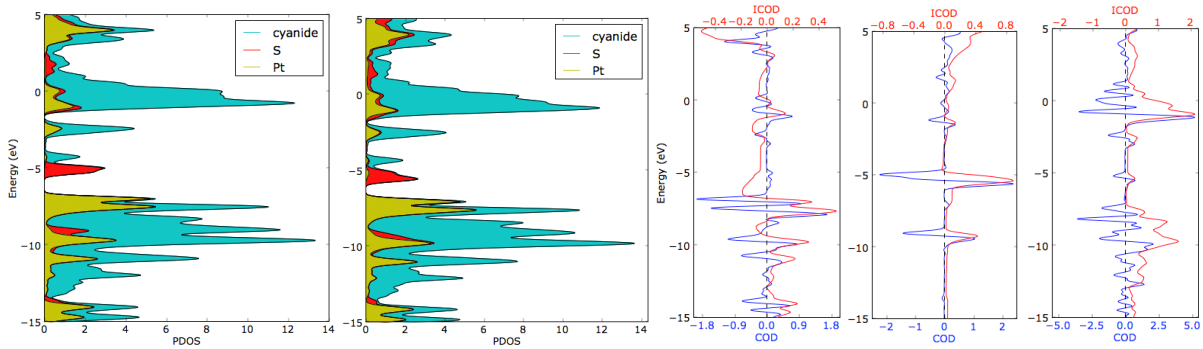
isolated host and guest host···guest Pt S CN